

Angle-dependent magic wavelengths for the $4s_{1/2} \rightarrow 3d_{5/2,3/2}$ transitions of Ca^+ ions

Jun Jiang,* Li Jiang, Z. W. Wu, Deng-Hong Zhang, Lu-You Xie, and Chen-Zhong Dong

Key Laboratory of Atomic and Molecular Physics and Functional Materials of Gansu Province,
College of Physics and Electronic Engineering, Northwest Normal University, Lanzhou 730070, P. R. China

(Dated: July 30, 2018)

The dynamic polarizabilities of the atomic states with angular momentum $j > \frac{1}{2}$ are sensitive to the angle between the quantization axis \hat{e}_z and the polarization vector $\hat{\epsilon}$ owing to the contribution of anisotropic tensor polarizabilities. The magic wavelength, at which the differential Stark shift of an atomic transition nullifies, depends on this angle. We identified the magic wavelengths for the $4s_{\frac{1}{2}} \rightarrow 3d_{\frac{3}{2},\frac{5}{2}}$ transitions of Ca^+ ions at different angles between \hat{e}_z and $\hat{\epsilon}$ in the case of linearly polarized light. We found that the magic wavelengths near 395.79 nm, which lie between the $4s_{\frac{1}{2}} \rightarrow 4p_{\frac{1}{2}}$ and $4s_{\frac{1}{2}} \rightarrow 4p_{\frac{3}{2}}$ transition wavelengths, remain insensitive to the angle, while the magic wavelengths, which are longer than the $3d_{\frac{5}{2}} \rightarrow 4p_{\frac{3}{2}}$ resonant transition wavelength (854.21 nm), are very sensitive to the angle.

I. INTRODUCTION

Techniques involving laser cooling and trapping of neutral atoms or ions have a lot of applications in quantum information [1–4], high-precision frequency and spectroscopy measurements [5, 6], and optical frequency standards [7–12]. However, the laser field can cause the Stark shifts. The problem of eliminating the Stark shifts can be solved by trapping an atom or ion at magic wavelengths, at which the Stark shifts of both the upper and lower states are the same and the shifts of the transition frequency vanish [13, 14]. Also, the systematic uncertainties of high-precision measurement can be reduced by optical trap at the magic wavelengths [15, 16]. In order to theoretically determine the magic wavelength of an atomic transition, accurate dynamic polarizabilities are required for the relevant atomic states, which consist of isotropic scalar and anisotropic vector and tensor parts [16–18]. The anisotropic parts result in a light shift, which depends on not only the angular momentum projection m but also the angle between the quantization axis \hat{e}_z and the electric polarization vector $\hat{\epsilon}$ of the laser. This will make accurate determinations of the magic wavelengths much difficult in experiments.

Due to the structure of energy-levels is simple and the $3d_{\frac{5}{2}}$ state has a long lifetime, calcium ions have been chosen as one of the candidates for optical frequency standard [19–26]. In a very recent experiment with a radio-frequency Paul trap, the accuracy of $^{40}\text{Ca}^+$ optical clocks has achieved a level of 3.4×10^{-17} [27]. In this experiment, excess micromotion was identified as the biggest factor affecting the accuracy of the $^{40}\text{Ca}^+$ clock [12]. If the weak micromotions of trapped ions can be handled, such kind of $^{40}\text{Ca}^+$ clocks could achieve a systematic fractional uncertainty of about 10^{-18} . Therefore, all-optical magic trapping of ions is worth of being tried for diminish substantially the micromotion-induced shifts [12, 15].

The magic wavelengths of Ca^+ ions have been studied extensively both in theory and experiment [15, 28, 29]. Two magic wavelengths of the $^{40}\text{Ca}^+$ $4s \rightarrow 3d_{\frac{5}{2}}$ ($m = \frac{1}{2}, \frac{3}{2}$) clock transitions near 395.79 nm for linearly polarized light have been measured with very high accuracy and they agree with all existing theoretical results very well [15, 28, 29]. However, these magic wavelengths are very close to the $4s_{\frac{1}{2}} \rightarrow 4p_{\frac{3}{2}}$ and $4s_{\frac{1}{2}} \rightarrow 4p_{\frac{1}{2}}$ resonant transition wavelengths which span from 393.366 nm to 396.847 nm. Therefore, they are not good for the use of magic trapping as the near-resonance light has high photon spontaneous scattering rates which result in a high heating process [30, 31]. Although many other magic wavelengths of Ca^+ ions were determined in theory, they were considered just in the situation of linearly polarized light with the quantization axis perpendicular to the wave vector ($\hat{e}_z \perp \hat{k}$) and parallel to the polarization vector ($\hat{e}_z \parallel \hat{\epsilon}$). To the best of our knowledge, the dependence of magic wavelengths upon the laser polarization direction has not been studied yet. The group in Wuhan Institute of Physics and Mathematics in China has tried to measure some other magic wavelengths with far-off resonance, but the results and theoretical values have a big difference [32].

In this paper, the magic wavelengths of Ca^+ ions for each of the magnetic sublevel components of the $4s_{\frac{1}{2}} \rightarrow 3d_{\frac{3}{2},\frac{5}{2}}$ transitions are identified for linearly polarized light based on our previous work [33]. The variations of the magic wavelengths with the applied laser direction are determined in detail. Finally, a brief summary is given in Sec. III. Atomic units, $\hbar = m = |e| = 1$, are used throughout this paper unless stated otherwise.

II. RESULTS AND DISCUSSION

The necessary atomic parameters of Ca^+ ions such as energy levels, matrix elements, and polarizabilities have been calculated by using the relativistic configuration interaction plus core polarization (RCICP) approach [34]

* phyjiang@yeah.net

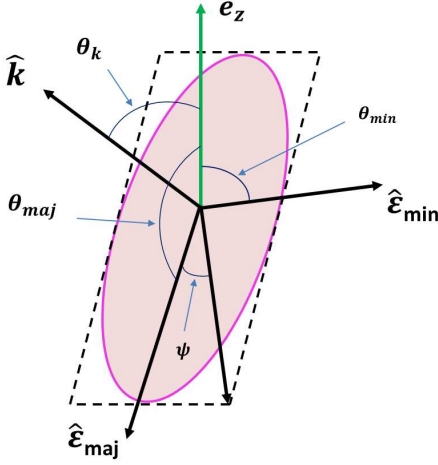


FIG. 1. Representation of the electromagnetic plane wave geometrical parameters. The surface represents the ellipse swept out by the electric field vector in one period. Unit vector \hat{e}_{maj} (\hat{e}_{min}) aligns with the semi-major (-minor) axis of the ellipse. The \hat{e}_z is quantization axis which selects the direction of magnetic field in experiment. The \hat{k} represents the direction of wave vector. The θ_k is angle between the \hat{e}_z and \hat{k} . Parameters \hat{e}_{maj} , \hat{e}_{min} and \hat{k} are mutually orthogonal. θ_{maj} (θ_{min}) is the angle between the \hat{e}_{maj} (\hat{e}_{min}) and the \hat{e}_z . Parameter ψ is directly related to the degree of circular polarization.

in our previous work [33]. These data are not repeated here for the sake of brevity.

For an arbitrarily polarized light, the dynamic polarizability of an atomic state i is given by [17, 18, 35]

$$\alpha_i(\omega) = \alpha_i^S(\omega) + \mathcal{A} \cos \theta_k \frac{m_{j_i}}{2j_i} \alpha_i^V(\omega) + \left(\frac{3 \cos^2 \theta_p - 1}{2} \right) \frac{3m_{j_i}^2 - j_i(j_i + 1)}{j_i(2j_i - 1)} \alpha_i^T(\omega), \quad (1)$$

where $\alpha_i^S(\omega)$, $\alpha_i^V(\omega)$, $\alpha_i^T(\omega)$ represent the scalar, vector, and tensor polarizabilities as given in Refs. [18, 36, 37], respectively; m_{j_i} is the component of total angular momentum j_i . There is no tensor polarizability for the states with $j \leq \frac{1}{2}$. θ_k is the angle between the wave vector k and the quantization axis \hat{e}_z , $\cos \theta_k = \hat{k} \cdot \hat{e}_z$. The relevant diagram is shown in Figure 1. The θ_p relates to the polarization vector \hat{e} and the \hat{e}_z axis. For a more general geometrical interpretation of θ_p , it is useful to further introduce the parameters θ_{maj} , θ_{min} , and ψ . $\cos^2 \theta_p$ can be written in the form [18]

$$\cos^2 \theta_p = \cos^2 \psi \cos^2 \theta_{maj} + \sin^2 \psi \cos^2 \theta_{min}, \quad (2)$$

where the parameter θ_{maj} (θ_{min}) is the angle between the major (minor) axis of the ellipse and the \hat{e}_z axis. From a geometrical consideration, θ_k and θ_p satisfy the relation $\cos^2 \theta_k + \cos^2 \theta_p \leq 1$ [17, 35]. The angle ψ is directly related to the degree of polarization of the light. \mathcal{A} represents the degree of polarization, which is give by

$$\mathcal{A} = \sin 2\psi. \quad (3)$$

In particular, $\mathcal{A} = 0$ corresponds to linear polarization, while $\mathcal{A} = +1$ (or -1) corresponds to right- (or left-) circular polarization. In experiment, however, \mathcal{A} could not absolutely be equal to zero. In this case, the vector polarizability contributes to the total dynamic polarizability. In order to get rid of the vector part in experiment, one can set $\cos \theta_k$ be equal to zero that is $\hat{e}_z \perp \hat{k}$.

For the case of $\cos \theta_k = 0$, the quantization axis \hat{e}_z is perpendicular to the wave vector \hat{k} , and the angle between the direction of polarization and \hat{e}_z varies in the plane of polarization. When $\mathcal{A} = 0$, or $\cos \theta_k = 0$, the dynamic polarizability can be easily simplified from Eq.(1) as follows,

$$\alpha_i(\omega) = \alpha_i^S(\omega) + \left(\frac{3 \cos^2 \theta_p - 1}{2} \right) \frac{3m_{j_i}^2 - j_i(j_i + 1)}{j_i(2j_i - 1)} \alpha_i^T(\omega)$$

The dynamic polarizability not only depends on the value of m but also the θ_p in a certain frequency ω .

In the case of $\cos \theta_k = 0$, parameters θ_{maj} and θ_{min} satisfy the relation

$$\theta_{maj} + \theta_{min} = \frac{\pi}{2}. \quad (5)$$

With the use of Eq. (3) and Eq. (5), Eq. (2) can be further simplified to

$$\cos^2 \theta_p = \frac{1}{2} + \frac{\sqrt{1 - \mathcal{A}^2}}{2} \cos 2\theta_{maj}. \quad (6)$$

Therefore, for a given value of \mathcal{A} , $\cos^2 \theta_p$ satisfies

$$\frac{1}{2} - \frac{\sqrt{1 - \mathcal{A}^2}}{2} \leq \cos^2 \theta_p \leq \frac{1}{2} + \frac{\sqrt{1 - \mathcal{A}^2}}{2}. \quad (7)$$

As seen from Eq. (7), $\mathcal{A} = 0$ corresponds to $0 \leq \cos^2 \theta_p \leq 1$, in which $\cos^2 \theta_p$ covers the largest range [0,1], while $|\mathcal{A}|=1$ just gives rise to $\cos^2 \theta_p = \frac{1}{2}$. In the following, we mainly discuss the case of linearly polarized light with $\cos \theta_k = 0$ which is numerically equivalent to $\mathcal{A} = 0$ as seen from Eq. (1).

Firstly, two particular cases are considered. One of them is $\cos^2 \theta_p = 1$. This means the \hat{e}_z axis is perpendicular to the wave vector but parallel to the polarization vector, i.e. $\hat{e}_z \perp \hat{k}$ and $\hat{e}_z \parallel \hat{e}$. In this case, Eq.(4) becomes

$$\alpha_i(\omega) = \alpha_i^S(\omega) + \frac{3m_{j_i}^2 - j_i(j_i + 1)}{j_i(2j_i - 1)} \alpha_i^T(\omega). \quad (8)$$

Another case is $\cos^2 \theta_p = 0$, which means the \hat{e}_z axis is perpendicular to the wave vector and the polarization vector, i.e. $\hat{e}_z \perp \hat{k}$ and $\hat{e}_z \perp \hat{e}$. Similarly, Eq.(4) is simplified as follows,

$$\alpha_i(\omega) = \alpha_i^S(\omega) - \frac{3m_{j_i}^2 - j_i(j_i + 1)}{2j_i(2j_i - 1)} \alpha_i^T(\omega). \quad (9)$$

Figure 2 shows the dynamic polarizabilities of the $4s$ and $3d_{\frac{5}{2}}$ states in the wavelength range 300 - 1400 nm for the laser polarization direction perpendicular (upper

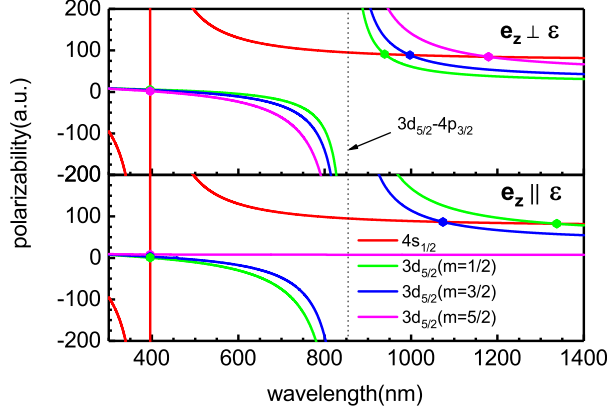


FIG. 2. Dynamic polarizabilities (in a.u.) of the $4s$ and $3d_{5/2}$ ($m = \frac{1}{2}, \frac{3}{2}, \frac{5}{2}$) states in the wavelength range 300 - 1400 nm. The upper panel plotted the dynamic polarizabilities in the case of $\hat{e}_z \perp \hat{\epsilon}$. The lower panel plotted the dynamic polarizabilities in the case of $\hat{e}_z \parallel \hat{\epsilon}$. The approximate position of the $3d_{5/2} \rightarrow 4p_{3/2}$ resonance is indicated by the vertical dotted line.

TABLE I. Magic wavelengths (nm) for the $4s_{1/2} - 3d_{5/2}$ transitions of the Ca^+ ions with the linearly polarized light. $\hat{e}_z \parallel \hat{\epsilon}$ represents the case that the \hat{e}_z axis is parallel the polarization vector $\hat{\epsilon}$. $\hat{e}_z \perp \hat{\epsilon}$ represents the case that the \hat{e}_z axis is perpendicular to the polarization vector $\hat{\epsilon}$.

RCICP	$\hat{e}_z \parallel \hat{\epsilon}$		RCICP
	DFCP [28]	R all-order [29]	
	$4s_{1/2} \rightarrow 3d_{5/2} (m=5/2)$		
			1179.33(57.92)
395.79485(4)	395.7968(1)	395.79	395.79608(9)
	$4s_{1/2} \rightarrow 3d_{5/2} (m=3/2)$		
1073.80(31.61)	1074.336(26.352)	1052.26	997.31(17.41)
395.79584(6)	395.7978(1)	395.79	395.79559(4)
	$4s_{1/2} \rightarrow 3d_{5/2} (m=1/2)$		
1337.31(115.38)	1338.474(82.593)	1271.92	938.83(8.97)
395.79633(11)	395.7982(1)	395.79	395.79534(1)

panel) and parallel (lower panel) the quantization axis, respectively. Since the dynamic polarizability of the $4s_{1/2}$ state only has the isotropic scalar part, the dynamic polarizability of the $4s_{1/2}$ state in case of $\hat{e}_z \perp \hat{\epsilon}$ is the same as the one in $\hat{e}_z \parallel \hat{\epsilon}$. However, the dynamic polarizabilities of the $3d_{5/2}$ state for both the cases $\hat{e}_z \perp \hat{\epsilon}$ and $\hat{e}_z \parallel \hat{\epsilon}$ are completely different for each magnetic components due to the contribution from the anisotropic tensor part. For example, when the wavelength is close to the $3d_{5/2} \rightarrow 4p_{3/2}$ resonant transition wavelength (854.21 nm), the dynamic polarizability of the $3d_{5/2} (m = \frac{5}{2})$ state is infinite in the case of $\hat{e}_z \perp \hat{\epsilon}$ but it is finite in the $\hat{e}_z \parallel \hat{\epsilon}$. To be more specific, as the explanation in Ref. [33], the contributions of the tensor and scalar terms from the $3d_{5/2} \rightarrow 4p_{3/2}$ transition cancel each other out in the case

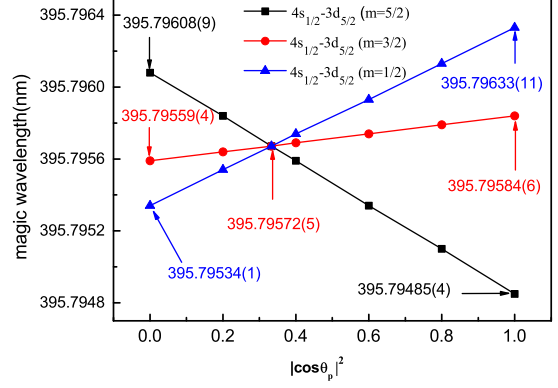


FIG. 3. The dependence of magic wavelengths, which lie between the $4s_{1/2} \rightarrow 4p_{1/2}$ transition wavelength (393.37 nm) and $4s_{1/2} \rightarrow 4p_{3/2}$ transition wavelength (396.85 nm), of each magnetic transition of the $4s_{1/2} \rightarrow 3d_{5/2}$ upon $\cos^2 \theta_p$ in the case of linearly polarized light.

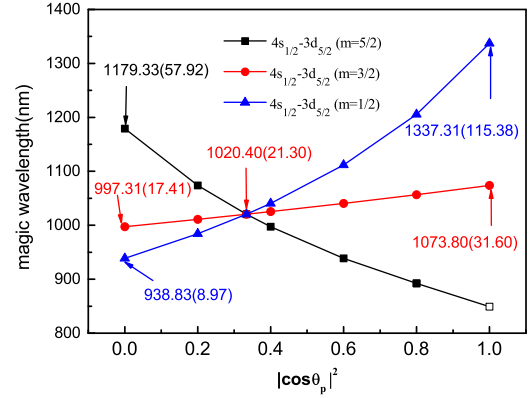


FIG. 4. Same as Fig 2 but for the magic wavelengths longer than the $3d_{5/2} \rightarrow 4p_{3/2}$ transition wavelength (854.21 nm).

of $\hat{e}_z \parallel \hat{\epsilon}$. The intersections of the dynamic polarizabilities of the $4s_{1/2}$ and each magnetic states of $3d_{5/2}$ give rise to magic wavelengths. For a given magnetic transition, we can see the magic wavelengths are different for the cases $\hat{e}_z \perp \hat{\epsilon}$ and $\hat{e}_z \parallel \hat{\epsilon}$. Two magic wavelengths have been found for each of $4s \rightarrow 3d_{5/2}$ magnetic transitions (except for the $4s \rightarrow 3d_{5/2} (m = 5/2)$ transition with $\hat{e}_z \parallel \hat{\epsilon}$, which only has one magic wavelength), one lies between $4s_{1/2} \rightarrow 4p_{1/2, 3/2}$ transition wavelengths, the other is longer than the $4p_{3/2} \rightarrow 3d_{5/2}$ transition wavelength (854.21nm).

Table I lists the magic wavelengths of the $4s_{1/2} \rightarrow 3d_{5/2}$ transition for the two particular cases, $\hat{e}_z \parallel \hat{\epsilon}$ and $\hat{e}_z \perp \hat{k}$, along with other available values. For the case of $\hat{e}_z \perp \hat{k}$, there are no existing results for comparison. It is found that the present results by using the RCICP approach are in good agreement with the results of Tang *et al.* [28] for the $\hat{e}_z \parallel \hat{\epsilon}$. The biggest difference is just 1.16 nm at 1337.31 nm. However, the results of Kaur *et al.* by using relativistic all-order method [29] have a big difference from the RCICP and Tang's results. For example, the

TABLE II. Magic wavelengths (nm) for the $4s_{\frac{1}{2}} - 3d_{\frac{3}{2}}$ transitions of the Ca^+ ions with the linearly polarized light.

	$\hat{e}_z \parallel \hat{\epsilon}$		$\hat{e}_z \perp \hat{\epsilon}$
RCICP	DFCP [28]	R all- order[29]	RCICP
	$4s_{\frac{1}{2}} \rightarrow 3d_{\frac{3}{2}}(m=3/2)$		
887.28(3.52)	887.382(3.196)	884.54	1142.81(44.52) 851.1325(78)
	$4s_{\frac{1}{2}} \rightarrow 3d_{\frac{3}{2}}(m=1/2)$		
395.7951(1)	395.7970(1)	395.79	395.79593(7)
1307.60(96.2)	1308.590(71.108)	1252.44	956.08(10.23)
850.3301(18)	850.335(2)	850.33	855.1243(560)
395.7962(1)	395.7981(1)	395.80	395.795381(2)

difference of the magic wavelengths between the RCICP and relativistic all-order results is 65.39 nm at 1337.31 nm, and 21.54 nm at 1073.80 nm.

Furthermore, we investigate the variation of magic wavelengths for the $4s \rightarrow 3d_{\frac{3}{2}}$ transition with $\cos^2\theta_p$. Figure 3 shows the dependence of the magic wavelengths near 395.79 nm upon $\cos^2\theta_p$, which lie between the $4s_{\frac{1}{2}} \rightarrow 4p_{\frac{1}{2}}$ and $4s_{\frac{1}{2}} \rightarrow 4p_{\frac{3}{2}}$ transition wavelengths. As shown clearly from Fig 3, the magic wavelengths change nearly linearly with $\cos^2\theta_p$. Also, the difference of magic wavelengths is small for different magnetic transitions. Meanwhile, the magic wavelength of each magnetic transition changes weakly with $\cos^2\theta_p$ as well. For example, for the $4s_{\frac{1}{2}} \rightarrow 3d_{\frac{5}{2}}(m = 5/2)$ transition, the difference of magic wavelengths is just 0.0012 nm for $\cos^2\theta_p = 0$ and $\cos^2\theta_p = 1$. The absolute values of derivatives of magic wavelengths for the $4s_{\frac{1}{2}} \rightarrow 3d_{\frac{5}{2}}(m = 1/2, 3/2, 5/2)$, $|d\lambda_{\text{magic}}/d\cos^2\theta_p|$, are 0.00099, 0.00025, 0.0012, respectively. It means these magic wavelengths are not sensitive to the quantity $\cos^2\theta_p$.

Figure 4 shows the dependence of the other magic wavelengths, which are longer than $3d_{\frac{3}{2}} \rightarrow 4p_{\frac{3}{2}}$ transition wavelength, for the $4s_{\frac{1}{2}} \rightarrow 3d_{\frac{3}{2}}$ transition upon $\cos^2\theta_p$. As seen from Fig 4, the magic wavelengths change nonlinearly. The magic wavelengths for the $4s_{\frac{1}{2}} \rightarrow 3d_{\frac{3}{2}}(m = 1/2, 3/2)$ transitions become longer with the increase of $\cos^2\theta_p$, while the magic wavelengths for the $4s_{\frac{1}{2}} \rightarrow 3d_{\frac{3}{2}}(m = 5/2)$ transition become shorter. Moreover, the magic wavelength of each magnetic transition changes strongly with $\cos^2\theta_p$. For example, for the $4s_{\frac{1}{2}} \rightarrow 3d_{\frac{3}{2}}(m = 1/2)$ transition, the difference of magic wavelengths is 398.48 nm for $\cos^2\theta_p = 0$ and $\cos^2\theta_p = 1$. The minimum absolute values of derivatives, $|d\lambda_{\text{magic}}/d\cos^2\theta_p|$, for the $4s_{\frac{1}{2}} \rightarrow 3d_{\frac{3}{2}}(m = 1/2, 3/2, 5/2)$ transitions are 228, 77, 217 respectively. Thence, these magic wavelength longer than the $3d_{\frac{3}{2}} \rightarrow 4p_{\frac{3}{2}}$ transition wavelength varies sensitively with $\cos^2\theta_p$.

As shown in Figures 3 and 4, however, different curves intersect at one point. The magic wavelength are independent of magnetic sublevels at the intersections. More-

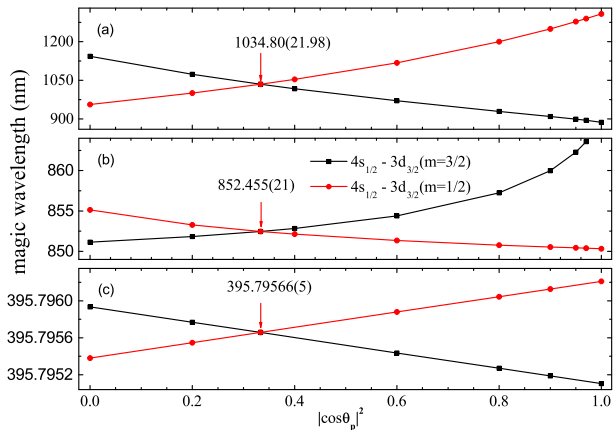


FIG. 5. The magic wavelengths of the $4s_{\frac{1}{2}} \rightarrow 3d_{\frac{3}{2}}$ transition of the Ca^+ ions for linearly polarized light. (a) the magic wavelengths which lie between the $4s_{\frac{1}{2}} \rightarrow 4p_{\frac{1}{2}}$ transition wavelength (393.37 nm) and $4s_{\frac{1}{2}} \rightarrow 4p_{\frac{3}{2}}$ transitions wavelength (396.85 nm); (b) the magic wavelengths which lie between the $3d_{\frac{3}{2}} \rightarrow 4p_{\frac{3}{2}}$ transition wavelength (849.80 nm) and $3d_{\frac{3}{2}} \rightarrow 4p_{\frac{1}{2}}$ transition wavelength (866.21 nm); (c) the magic wavelengths longer than the $3d_{\frac{3}{2}} \rightarrow 4p_{\frac{1}{2}}$ transition wavelength (866.21 nm).

over, at the intersections, the contribution of tensor polarizabilities is zero. This condition can be attained when $\cos^2\theta_p = \frac{1}{3}$ for a linearly polarized light. Under this condition, the angle θ_p is referred to as "magic angle" [38] and is given by

$$\theta_p = \arccos\left(\frac{1}{\sqrt{3}}\right) \approx 54.74^\circ. \quad (10)$$

According to Eq. (7), the determination of the "magic angle" requires the condition $|\mathcal{A}| \leq \frac{2\sqrt{2}}{3}$. The magic wavelengths corresponding to the magic angle are determined for the $4s_{\frac{1}{2}} \rightarrow 3d_{\frac{3}{2}}$ transition as shown in Figures 3 and 4. For instance, at the magic angle, the magic wavelength are 395.79572(5) and 1024.40(21.30) nm for the $4s_{\frac{1}{2}} \rightarrow 3d_{\frac{3}{2}}$ transition.

Table II lists the magic wavelengths for the $4s_{\frac{1}{2}} \rightarrow 3d_{\frac{3}{2}}$ transition in the cases of $\hat{e}_z \parallel \hat{\epsilon}$ and $\hat{e}_z \perp \hat{\epsilon}$. Good consistency is obtained for the $\hat{e}_z \parallel \hat{\epsilon}$, while there are currently no comparable results for $\hat{e}_z \perp \hat{\epsilon}$. Figure 5 shows the dependence of the magic wavelengths for the $4s_{\frac{1}{2}} \rightarrow 3d_{\frac{3}{2}}$ transition upon $\cos^2\theta_p$. Similarly, the magic wavelength near 395.79 nm is insensitive to $\cos^2\theta_p$, while the magic wavelength longer than 854.21 nm strongly depends on $\cos^2\theta_p$.

III. CONCLUSIONS

The dynamic polarizabilities of the $4s_{\frac{1}{2}}$ and $3d_j$ states of the Ca^+ ions are calculated. The magic wavelengths

for the $4s_{\frac{1}{2}} \rightarrow 3d_{\frac{3}{2},\frac{5}{2}}$ transitions are identified for $\hat{e}_z \perp \hat{\epsilon}$ and $\hat{e}_z \parallel \hat{\epsilon}$ in the case of a linearly polarized light ($\cos\theta_k = 0$ or $\mathcal{A} = 0$). The dependence of the magic wavelengths upon the $\cos^2\theta_p$ are analyzed. It is found that the magic wavelength near 395.79 nm is insensitive to the angle between the quantization axis \hat{e}_z and the polarization vector $\hat{\epsilon}$. In contrast, the magic wavelength longer than the $3d_{\frac{5}{2}} \rightarrow 4p_{\frac{3}{2}}$ transition wavelength (854.21 nm) is very sensitive to $\cos^2\theta_p$ due to the contribution of the anisotropic tensor polarizability. Meanwhile, we find that some particular magic wavelengths are independent of magnetic sublevels at the magic angle.

IV. ACKNOWLEDGMENTS

This work was supported by the National Key Research and Development Program of China under Grant No.2017YFA0402300 and National Natural Science Foundation of China (NSFC) (Grant Nos.11564036, 11774292, U1530142, 11464042) and the Young Teachers Scientific Research Ability Promotion Plan of Northwest Normal University (NWNLU-LKQN-15-3).

-
- [1] T. G. Tiecke, J. D. Thompson, N. P. de Leon, L. R. Liu, V. Vuletić, and M. D. Lukin, *Nature* **508**, 241 (2014).
- [2] H. Häffner, C. Roos, and R. Blatt, *Physics Reports* **469**, 155 (2008).
- [3] G. Wilpers, C. W. Oates, S. A. Diddams, A. Bartels, T. M. Fortier, W. H. Oskay, J. C. Bergquist, S. R. Jefferts, T. P. Heavner, T. E. Parker, et al., *Metrologia* **44**, 146 (2007).
- [4] C. Monroe, D. M. Meekhof, B. E. King, W. M. Itano, and D. J. Wineland, *Phys. Rev. Lett.* **75**, 4714 (1995).
- [5] S. N. Lea, *Reports on Progress in Physics* **70**, 1473 (2007).
- [6] C. S. Wood, S. C. Bennett, D. Cho, B. P. Masterson, J. L. Roberts, C. E. Tanner, and C. E. Wieman, *Science* **275**, 1759 (1997).
- [7] A. D. Ludlow, T. Zelevinsky, G. K. Campbell, S. Blatt, M. M. Boyd, M. H. G. de Miranda, M. J. Martin, J. W. Thomsen, S. M. Foreman, J. Ye, et al., *Science* **319**, 1805 (2008).
- [8] T. Rosenband, D. B. Hume, P. O. Schmidt, C. W. Chou, A. Brusch, L. Lorini, W. H. Oskay, R. E. Drullinger, T. M. Fortier, J. E. Stalnaker, et al., *Science* **319**, 1808 (2008).
- [9] N. Hinkley, J. A. Sherman, N. B. Phillips, M. Schioppo, N. D. Lemke, K. Beloy, M. Pizzocaro, C. W. Oates, and A. D. Ludlow, *Science* **341**, 1215 (2013).
- [10] Y. Huang, J. Cao, P. Liu, K. Liang, B. Ou, H. Guan, X. Huang, T. Li, and K. Gao, *Phys. Rev. A* **85**, 030503 (2012).
- [11] M. Takamoto, F.-L. Hong, R. Higashi, and H. Katori, *Nature* **435** (2005).
- [12] Y. Huang, H. Guan, P. Liu, W. Bian, L. Ma, K. Liang, T. Li, and K. Gao, *Phys. Rev. Lett.* **116**, 013001 (2016).
- [13] J. Ye, D. W. Vernooy, and H. J. Kimble, *Phys. Rev. Lett.* **83**, 4987 (1999).
- [14] H. Katori, T. Ido, and M. K. Gonokami, *J. Phys. Soc. Jpn.* **68**, 2479 (1999).
- [15] P.-L. Liu, Y. Huang, W. Bian, H. Shao, H. Guan, Y.-B. Tang, C.-B. Li, J. Mitroy, and K.-L. Gao, *Phys. Rev. Lett.* **114**, 223001 (2015).
- [16] J. Hendrik Becher, S. Baier, K. Aikawa, M. Lepers, J.-F. Wyart, O. Dulieu, and F. Ferlaino, *ArXiv e-prints* (2017), 1710.07162.
- [17] N. L. Manakov, V. D. Ovsiannikov, and L. P. Rapoport, *Physics Reports* **141**, 320 (1986).
- [18] K. Beloy, Ph.D. thesis, University of Nevada (2009).
- [19] M. Chwalla, J. Benhelm, K. Kim, G. Kirchmair, T. Monz, M. Riebe, P. Schindler, A. S. Villar, W. Hänsel, C. F. Roos, et al., *Phys. Rev. Lett.* **102**, 023002 (2009).
- [20] K. Matsubara, H. Hachisu, Y. Li, S. Nagano, C. Locke, A. Nogami, M. Kajita, K. Hayasaka, T. Ido, and M. Hosokawa, *Opt. Express* **20**, 22034 (2012).
- [21] H. C. Nägerl, C. Roos, D. Leibfried, H. Rohde, G. Thalhammer, J. Eschner, F. Schmidt-Kaler, and R. Blatt, *Phys. Rev. A* **61**, 023405 (2000).
- [22] A. Kreuter, C. Becher, G. P. T. Lancaster, A. B. Mundt, C. Russo, H. Häffner, C. Roos, W. Hänsel, F. Schmidt-Kaler, R. Blatt, et al., *Phys. Rev. A* **71**, 032504 (2005).
- [23] P. A. Barton, C. J. S. Donald, D. M. Lucas, D. A. Stevens, A. M. Steane, and D. N. Stacey, *Phys. Rev. A* **62**, 032503 (2000).
- [24] B. Arora, M. S. Safronova, and C. W. Clark, *Phys. Rev. A* **76**, 064501 (2007).
- [25] C. Champenois, M. Houssin, C. Lisowski, M. Knoop, G. Hagel, M. Vedel, and F. Vedel, *Physics Letters A* **331**, 298 (2004), ISSN 0375-9601.
- [26] M. Kajita, Y. Li, K. Matsubara, K. Hayasaka, and M. Hosokawa, *Phys. Rev. A* **72**, 043404 (2005).
- [27] Y. Huang, H. Guan, P. Liu, W. Bian, L. Ma, K. Liang, T. Li, and K. Gao, *Phys. Rev. Lett.* **116**, 013001 (2016).
- [28] Y.-B. Tang, H.-X. Qiao, T.-Y. Shi, and J. Mitroy, *Phys. Rev. A* **87**, 042517 (2013).
- [29] J. Kaur, S. Singh, B. Arora, and B. K. Sahoo, *Phys. Rev. A* **92**, 031402 (2015).
- [30] D. L. Haycock, S. E. Hamann, G. Klose, and P. S. Jessen, *Phys. Rev. A* **55**, R3991 (1997).
- [31] T. A. Savard, K. M. O'Hara, and J. E. Thomas, *Phys. Rev. A* **56**, R1095 (1997).
- [32] K.-L. Gao, private communication (2017).
- [33] J. Jiang, L. Jiang, X. Wang, D.-H. Zhang, L.-Y. Xie, and C.-Z. Dong, *Phys. Rev. A* **96**, 042503 (2017).
- [34] J. Jiang, J. Mitroy, Y. Cheng, and M. W. J. Bromley, *Phys. Rev. A* **94**, 062514 (2016).
- [35] F. Le Kien, P. Schneeweiss, and A. Rauschenbeutel, *Eur. Phys. J. D* **67**, 92 (2013).
- [36] F. Le Kien, P. Schneeweiss, and A. Rauschenbeutel, *Eur. Phys. J. D* **67**, 92 (2013).
- [37] N. L. Manakov, V. D. Ovsiannikov, and L. P. Rapoport, *Physics Reports* **141**, 320 (1986).
- [38] D. Budker, D. F. Kimball, and D. P. DeMille, *Atomic physics: An exploration through problems and solutions* (Oxford University Press, 2004).